Bioconjugate Chemistry

pubs.acs.org/bc

Article

Synthetic Tuning of Domain Stoichiometry in Nanobody−Enzyme Megamolecules

Kevin J. Metcalf,[†] Blaise R. Kimmel,[†] Daniel J. Sykora, Justin A. Modica, Kelly A. Parker, Eric Berens, Raymond Dai, Vinayak P. Dravid, Zena Werb, and Milan Mrksich*

Cite This: https://dx.doi.org/10.1021/acs.bioconjchem.0c00578

Read Online

ACCESS | Metrics & More | Article Recommendations | Supporting Information

ABSTRACT: This paper presents a method to synthetically tune atomically precise megamolecule nanobody−enzyme conjugates for prodrug cancer therapy. Previous efforts to create heterobifunctional protein conjugates suffered from heterogeneity in domain stoichiometry, which in part led to the failure of antibody−enzyme conjugates in clinical trials. We used the megamolecule approach to synthesize anti-HER2 nanobody−cytosine deaminase conjugates with tunable numbers of nanobody and enzyme domains in a single, covalent molecule. Linking two nanobody domains to one enzyme domain improved avidity to a human cancer cell line by 4-fold but did not increase cytotoxicity significantly due to lowered enzyme activity. In contrast, a megamolecule composed of one nanobody and two enzyme domains resulted in an 8-fold improvement in the catalytic efficiency and increased the cytotoxic effect by over 5-fold in spheroid culture, indicating that the multimeric structure allowed for an increase in local drug activation. Our work demonstrates that the megamolecule strategy can be used to study structure−function relationships of protein conjugate therapeutics with synthetic control of protein domain stoichiometry.

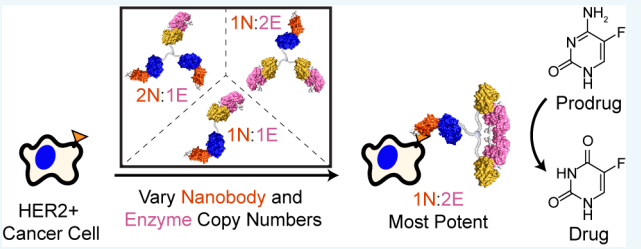

INTRODUCTION

Many chemotherapy drugs target cancer cells due to their proliferative growth. However, proliferative noncancer cells are also affected, resulting in the death of healthy cell populations and severe side-effects for patients. Local delivery of chemotherapeutics to tumors could improve patient care and treatment outcomes. One strategy to achieve local delivery of chemotherapeutics is antibody-directed enzyme prodrug therapy (ADEPT).[1] This strategy employs a heterobifunctional antibody−enzyme conjugate that specifically binds to a tumor-specific antigen and enzymatically activates a nontoxic prodrug into a toxic chemotherapeutic within the tumor microenvironment (Figure 1A).[2,3] Synthesis of the antibody−enzyme conjugate requires the antibody and enzyme domains to be covalently joined.[4,5] However, previous approaches to synthesize antibody−enzyme conjugates yielded heterogeneous conjugates, making it difficult to investigate structure−function relationships and leading to stalled early-stage translation.[6]

Homogeneous covalent protein conjugation is a key to the design of an antibody−enzyme conjugate, where cross-linking specific amino acid residues results in a homogeneous structure. Bioconjugation strategies that use naturally occurring reactive amino acids (e.g., cysteine and lysine)[7] or unnatural reactive amino acids (e.g., azide-, alkyne-, or aldehyde-containing amino acids)[8] are routinely employed for this purpose. However, conjugation using naturally occurring reactive amino acids often results in heterogeneous conjugation and incorporation of unnatural reactive amino acids can be inefficient.[9,10]

Here, we synthesized megamolecules—homogeneous protein nanostructures—that possess both cancer cell-binding and prodrug-activating domains. Megamolecules are assembled from fusion proteins and linkers, where reactions of enzyme domains with irreversible inhibitors on the linker are used to assemble larger molecules in a modular fashion.[11−14] We synthesized nanobody−enzyme megamolecules, which are composed of a prodrug-activating enzyme and a cancer-cell-targeting nanobody. The enzyme, yeast cytosine deaminase (yCD), activates the nontoxic 5-fluorocytosine (5-FC) into the chemotherapeutic 5-fluorouracil (5-FU), making it well-suited for antibody-directed enzyme prodrug therapy.[15] Because the active form of yCD is a homodimer, the yCD fusion protein must dimerize to form a fully active enzyme.

As a proof-of-concept system, we targeted HER2+ breast cancer. To deliver yCD to HER2+ cancer cells, we employed the anti-HER2 nanobody 5F7, which comes from the variable region of an engineered camelid heavy-chain antibody that was previously generated using phage display from SK-BR-3 immunized llamas.[16,17] A nanobody has the advantages of being recombinantly expressed in *Escherichia coli* and having

Received: October 22, 2020
Revised: November 24, 2020

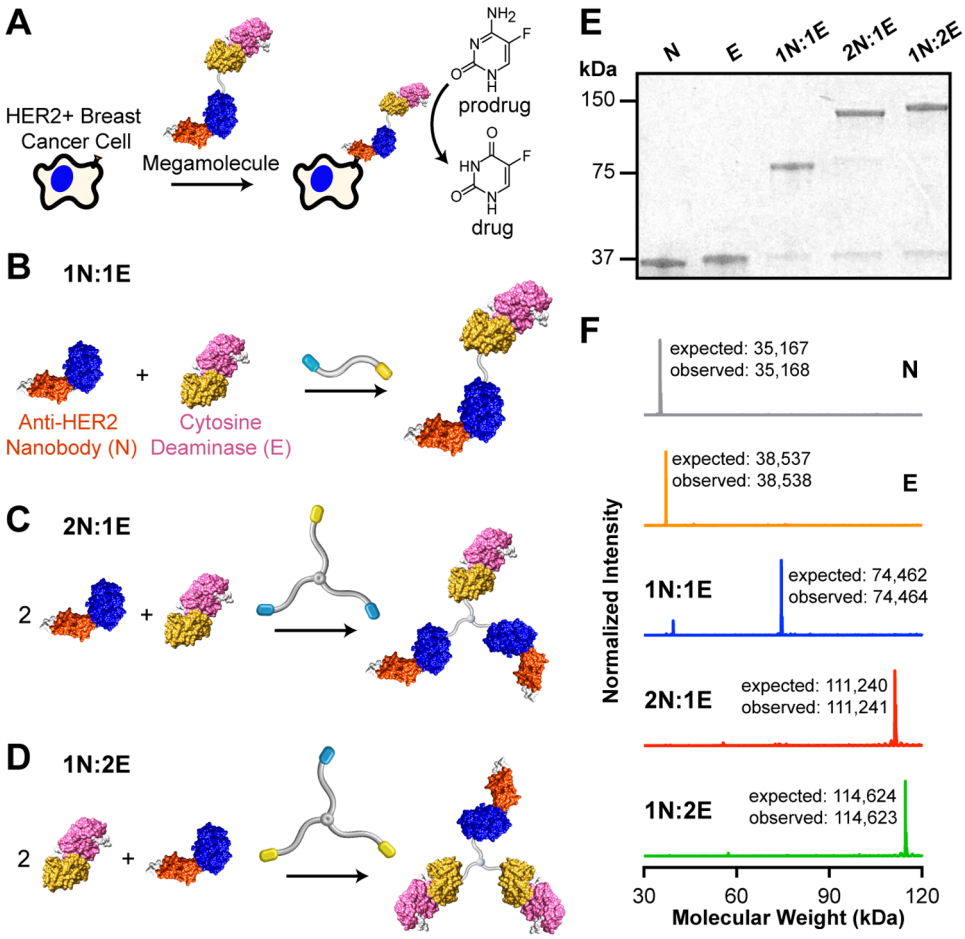

Figure 1. Design and synthesis of nanobody−enzyme megamolecules. A. Scheme of a nanobody−enzyme megamolecule binding to a HER2+ cancer cell followed by activation of the nontoxic prodrug 5-FC into the chemotherapeutic drug 5-FU. B. The anti-HER2 nanobody "N" (orange) is fused to the cutinase (blue) protein, and the yeast cytosine deaminase enzyme "E" (pink) is fused to the SnapTag (yellow) protein. The two fusion proteins are conjugated by use of a heterobifunctional linker, which is terminated by a *p*-nitrophenyl phosphonate group (blue) and a benzyl chloropyrimidine group (yellow). C,D. Reaction schemes for multidomain megamolecule syntheses using trifunctional linkers: C, 2N:1E; D, 1N:2E. E. SDS-PAGE characterization of fusion proteins and SEC-purified megamolecules. F. Deconvoluted mass spectra of purified megamolecules.

improved tumor penetration when compared to a monoclonal antibody.[18] We hypothesized that the efficacy of nanobody-directed enzyme prodrug therapy depends on the structure of the nanobody−enzyme conjugate. We tested this hypothesis by synthesizing nanobody−enzyme megamolecules with an increasing number of nanobody or enzyme domains. Homogeneous megamolecules containing tunable numbers of nanobody and enzyme domains for prodrug cancer therapy allows us to address the role of stoichiometry—particularly as it relates to bivalent binding to the cell surface and dimerization of the enzyme—and enables the synthesis of homogeneous antibody conjugates for structure−function studies of therapeutic efficacy of next-generation biologics for cancer therapy.[19−23]

RESULTS

Design and Synthesis of Nanobody−Enzyme Megamolecules. We synthesized nanobody−enzyme megamolecules with the megamolecule approach, where fusion proteins—containing either the nanobody or enzyme domains—react covalently with small molecule cross-linkers (Figure 1B). The fusion proteins possess two domains: a functional domain (either the nanobody for binding or the enzyme for prodrug activation) and a linking domain (either cutinase or SnapTag).[24,25] Fusion proteins were produced in *E. coli* and purified by affinity chromatography (Figure 1E,F). The cross-linkers are terminated with substrates that covalently bind to the nucleophilic residues in the active site of either linking domain and are orthogonally reactive in solution.[11,12]

We used a *p*-nitrophenyl phosphonate (pNPP) functional group for reactions with cutinase and a benzyl-2-chloro-6-aminopyrimidine (CP) functional group for reactions with SnapTag.[11,12,26] We synthesized a megamolecule having one nanobody domain and one enzyme domain (1N:1E) by joining the two fusion proteins with a linker possessing an undecyl ethylene glycol (EG11) core terminated with one pNPP group and one CP group, as previously reported.[12−14] The proteins were prepared by fusing cutinase and the 5F7 anti-HER2 nanobody (N) (cutinase-N)[16] as well as SnapTag and yCD (E) (SnapTag-E).[27] The purified 1N:1E megamolecule was >80% pure as determined by SDS-PAGE and intact protein mass spectrometry (ESI-MS) (Figure 1E,F and Figure S1). We identified by ESI-MS that the contaminating species was unreacted E fusion protein that coelutes with megamolecules, because it runs as a homodimer by SEC. We did not observe the formation of any other products, indicating the chemoselectivity of this conjugation reaction. Attempts to cross-link nanobody

https://dx.doi.org/10.1021/acs.bioconjchem.0c00578
Bioconjugate Chem. XXXX, XXX, XXX−XXX

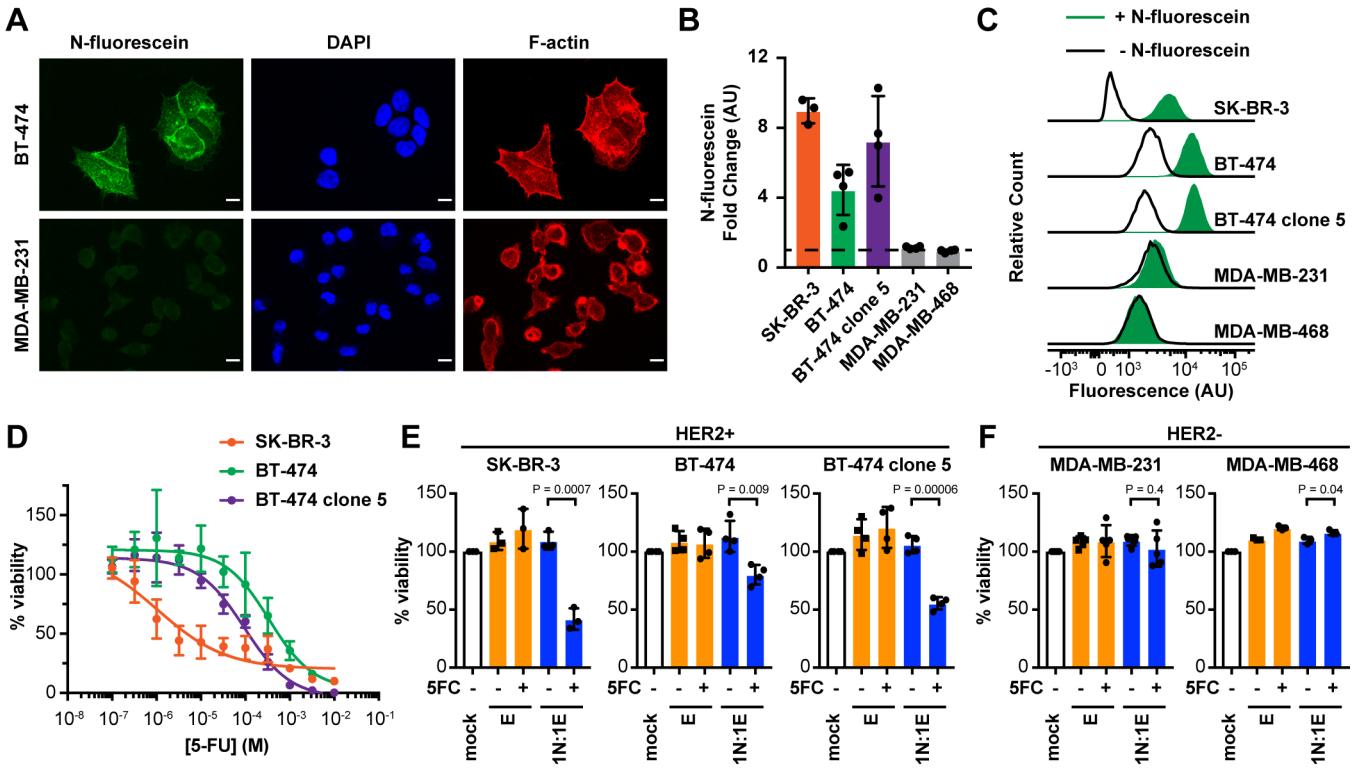

Figure 2. Characterization of nanobody and enzyme activities of the 1N:1E megamolecule. A. Immunofluorescence images of adherent cells stained for HER2 (cutinase-nanobody), nucleus (DAPI), and cytoskeleton (F-actin). Scale bar is 10 μm. B. Plot of median fluorescence intensity ratio measured by flow cytometry of cell lines treated with fluorescently labeled cutinase−nanobody fusion protein (+N-fluorescein) divided by untreated cells (−N-fluorescein). An MFI ratio of 1 signifies no binding interaction and is represented by a horizontal dashed line. C. Representative flow cytometry histograms used to calculate the values in panel B. D. Plots of 5-FU dose−response titrations for HER2+ cell lines in adherent culture. E,F. Plots of cell viability after treatment for E, HER2+ and F, HER2− cell lines with 10 nM of the enzyme (E) or 1N:1E megamolecule (1N:1E), washing, and then 5-FC or vehicle. The concentrations of 5-FC were equal to 10 times the IC_{50} for each cell line, according to Table 1. Mock treatment is represented by 100% viability. The mean of 3−4 biologic replicates is plotted and the error bars represent 1 standard deviation.

and enzyme using a lysine-to-cysteine cross-linker (succinimidyl 4-(*N*-maleimidomethyl)cyclohexane-1-carboxylate, SMCC) resulted in a heterogeneous mixture with varying domain numbers and conjugation sites (Figure S2), in contrast to the homogeneity of domain number and conjugation sites seen in the 1N:1E megamolecule.

We used the megamolecule approach to also prepare molecules having more than one copy of the nanobody or enzyme domain. We used a previously reported linker that has two CP groups and one pNPP group on an EG11 backbone (CP/CP/pNPP)[28] to form a 1N:2E megamolecule (1 nanobody domain and 2 enzyme domains), and a new linker that had two pNPP groups and one CP group on an EG11 backbone (pNPP/pNPP/CP) to produce a 2N:1E megamolecule (2 nanobody domains and 1 enzyme domain) (Figure 1C,D). Analysis of the purified megamolecules by SDS-PAGE and mass spectrometry for 2N:1E and 1N:2E megamolecules confirmed a single homogeneous product for each reaction (Figure 1E,F).

Evaluation of 1N:1E Megamolecule Cell Binding and Drug Activation. To confirm that the nanobody and enzyme domains remained functional in the megamolecule, we measured their activities independently. We tested the megamolecule against a panel of human breast cancer cell lines for assessing the specificity and cytotoxicity of nanobody−enzyme megamolecule prodrug therapy. These cell lines differed in their HER2 expression level, where one group of cells overexpressed HER2 (SK-BR-3, BT-474, and BT-474 clone 5) and a second group was HER2- (MDA-MB-231 and MDA-MB-468).[29] We first tested the specificity of the nanobody to bind to HER2+ human breast cancer cell lines. To demonstrate that the N fusion protein binds to the membrane of the HER2+ cell line BT-474 but not to the HER2- cell line MDA-MB-231, we labeled the N fusion protein with fluorescein (Figure 2A). Against a panel of human breast cancer cell lines, the N fusion protein bound to all HER2+ cell lines (SK-BR-3, BT-474, and BT-474 clone 5) and to none of the HER2− cell lines (MDA-MB-231 and MDA-MB-468) (Figure 2B,C and Figure S3). These results show that the N fusion protein binds specifically to HER2+ human breast cancer cell lines.

We also tested the cytotoxic effect of 5-FC and 5-FU for each of the cell lines. Each of these cell lines was not sensitive to the prodrug 5-FC and sensitive to the chemotherapeutic 5-FU (Figure 2D and Figure S4). The 5-FU IC_{50} values for each cell line varied over 2 orders of magnitude, with BT-474 the most resistant cell line and SK-BR-3 the most sensitive cell line (Figure 2D and Table 1). The BT-474 clone 5 cell line, which is resistant to anti-HER2 antibody treatment (Figure S5),[30] was sensitive to 5-FU treatment (Figure 2D).

Compared to adherent culture, spheroid cultures better model tumor structure and drug penetration.[31−34] We therefore tested the cytotoxicity of 5-FC and 5-FU in spheroid culture. Only the BT-474 and BT-474 clone 5 cell lines formed spheroids (Figure S6).[35] While BT-474 was similarly sensitive to 5-FU treatment in adherent and spheroid culture, BT-474 clone 5 was more resistant to 5-FU treatment in spheroid culture (Figure S7 and Table 1), an effect observed in previous studies.[36,37] To

https://dx.doi.org/10.1021/acs.bioconjchem.0c00578
Bioconjugate Chem. XXXX, XXX, XXX−XXX

Table 1. Fitted IC_{50} Values for Each Cell Line Treated with 5-FU[a]

cell line	HER2 status[29]	culture format	IC_{50} (μM)
SK-BR-3	+++	adherent	1.1 ± 1.5
BT-474	+++	adherent	340 ± 150
BT-474	+++	spheroid	370 ± 150
BT-474 clone 5	+++	adherent	95 ± 20
BT474 clone 5	+++	spheroid	160 ± 40
MDA-MB-231	-	adherent	98 ± 15
MDA-MB-468	-	adherent	4.3 ± 1.9

[a]Error represents the standard error of fitting.

enable comparison between cell lines, all remaining experiments used a concentration of 5-FC set to ten times the 5-FU IC_{50}, unless otherwise noted.

To validate that enzyme function was retained after incorporation into a megamolecule, we tested cytotoxicity upon combination treatment of the 1N:1E megamolecule and 5-FC without washing to remove unbound protein. For all cell lines tested, the cytotoxicity of the 1N:1E megamolecule and 5-FC combination treatment was similar to 5-FU treatment, indicating the yCD domain in the 1N:1E megamolecule converts 5-FC to 5-FU (Figure S8).

We then tested the ability of the megamolecule to bind cells and activate drug simultaneously using a two-step treatment. We first incubated cells with the E fusion protein or the 1N:1E megamolecule. Next, we washed the plate to remove unbound protein. Then, we added 5-FC or vehicle to cells and measured cell viability after 5 days. For all HER2+ cell lines, only the two-step treatment of the 1N:1E megamolecule and 5-FC resulted in cytotoxicity, indicating that the 1N:1E megamolecule both bound to these cells and activated 5-FC (Figure 2E). To test the specificity of this interaction, we repeated the same experiment with HER2− cell lines. The two-step treatment with the 1N:1E megamolecule and 5-FC was not cytotoxic for HER2− cell lines, indicating that cytotoxicity requires binding of the 1N:1E megamolecule via HER2 (Figure 2F). For both the HER+ and HER2− cell lines, the E fusion protein did not produce a cytotoxic effect because it does not bind to cells. Thus, nanobody−enzyme megamolecules retain cell-binding and 5-FC-activating activities of the individual domains. Further, these activities are achieved simultaneously.

Characterizing Megamolecule Multimericity. The yCD fusion protein contained a single domain; however, the enzyme assembles into a homodimer in solution,[38] and the effect of multimericity on the solution-phase structure of megamolecules was not known. The 1N:2E megamolecule possess two yCD domains, allowing for intramolecular dimerization in a single megamolecule. In contrast, the 1N:1E and 2N:1E megamolecules each contain one yCD domain, requiring intermolecular dimerization (Table S1). Accordingly, we tested megamolecule dimerization using several methods.

We first characterized the multimeric state of the megamolecules using size-exclusion chromatography (SEC). Based on calibration with globular protein standards, only the N fusion protein and the 1N:2E megamolecule permeated the column as globular proteins, indicating a monomeric structure. In contrast, the E fusion protein and the 1N:1E and 2N:1E megamolecules exhibited shorter retention times than predicted for monomers. When we assumed an intermolecular dimer for these three molecules, the megamolecules permeated the column as globular proteins, supporting a dimeric structure (Figure 3A and Figure S9). Given the differences in inter- versus intramolecular enzyme dimerization, we next characterized the enzyme activity of the E fusion protein and the 1N:1E and 1N:2E megamolecules. We determined the Michaelis−Menten parameters of E, 1N:1E, and 1N:2E and saw the largest catalytic efficiency (k_{cat}/K_M) in the 1N:2E megamolecule and the smallest catalytic efficiency in the 1N:1E megamolecule (Figure 3B). The calculated values of K_M and k_{cat} for the E fusion protein agree well with previously reported values for yCD of 0.16 ± 0.01 mM and 17 ± 0.4 s^{-1}, respectively.[39] We found that the 1N:2E megamolecule had the highest catalytic efficiency, suggesting that the intramolecular dimerization increased enzyme activity.

Because the E fusion protein and the 1N:1E and 2N:1E megamolecules formed intermolecular dimers, we varied protein concentration and measured enzyme activity to determine the enzyme dissociation constant, $K_{D,E}$. We used a model that assumes the dimeric form has greater activity than the monomer, resulting in lower activity at concentrations below the dimer $K_{D,E}$.[40,41] This model predicts quadratic behavior at enzyme concentrations below $K_{D,E}$. At low protein concentrations, the relationship between the protein concentration and enzyme activity of the E fusion protein and the 1N:1E megamolecule was nonlinear, while the 1N:2E megamolecule was linear (Figure 3C). The calculated value of $K_{D,E}$ was 12 ± 7 μM and 38 ± 26 μM for the E fusion protein and 1N:1E megamolecule, respectively. No value of $K_{D,E}$ was calculated for the 1N:2E megamolecule. These results are consistent with an active intermolecular dimer for the E fusion protein and the 1N:1E megamolecule, and an active intramolecular dimer for the 1N:2E megamolecule.

Finally, we obtained direct images of the megamolecules with transmission electron microscopy (TEM). The images revealed dimer lengths of 14 nm ± 2 nm for E, 18 nm ± 4 nm for 1N:1E, 11 nm ± 2 nm for 1N:2E, and 16 nm ± 3 nm for 2N:1E (Figure 3D and Figure S10). The variation in megamolecule size between images arises from differences in the orientation and folding when complex structures deposit and dry on the grid, as well as from the approximately 1 nm resolution limit from the uranyl formate negative stain.[42] Negative staining leads to structure breakup because of the harsh non-native pH condition, so representative intact structures were used for this analysis. Additional examples of each structure are included in the Supporting Information (Figure S10). TEM imaging also revealed that megamolecules are conformationally flexible, which is consistent with our previous work.[13,28] Based on the relative sizes, these images confirm that the 1N:2E megamolecule was monomeric, while the 1N:1E and 2N:1E megamolecules were dimeric (Table S1).

Dynamics of Megamolecule Binding and Penetration. We next quantified megamolecule binding affinity to HER2+ cell lines. We synthesized a nanobody−fluorescent protein megamolecule using superfolder green fluorescent protein (sfGFP) (1N:1GFP) as a surrogate structure for 1N:1E. We cloned a SnapTag-sfGFP fusion protein and cross-linked the fluorescent fusion protein to the N fusion protein using the same heterobifunctional linker as used in the synthesis of 1N:1E, forming a 1N:1GFP megamolecule (Figure 4A and Figure S11). Notably, because sfGFP exists as a stable monomer at the concentrations used in this study, we did not expect fluorescent megamolecule dimerization.[43]

The 1N:1GFP megamolecule bound to the HER2+ BT-474 cell line, but not the HER2− MDA-MB-231 cell line (Figure

https://dx.doi.org/10.1021/acs.bioconjchem.0c00578
Bioconjugate Chem. XXXX, XXX, XXX−XXX

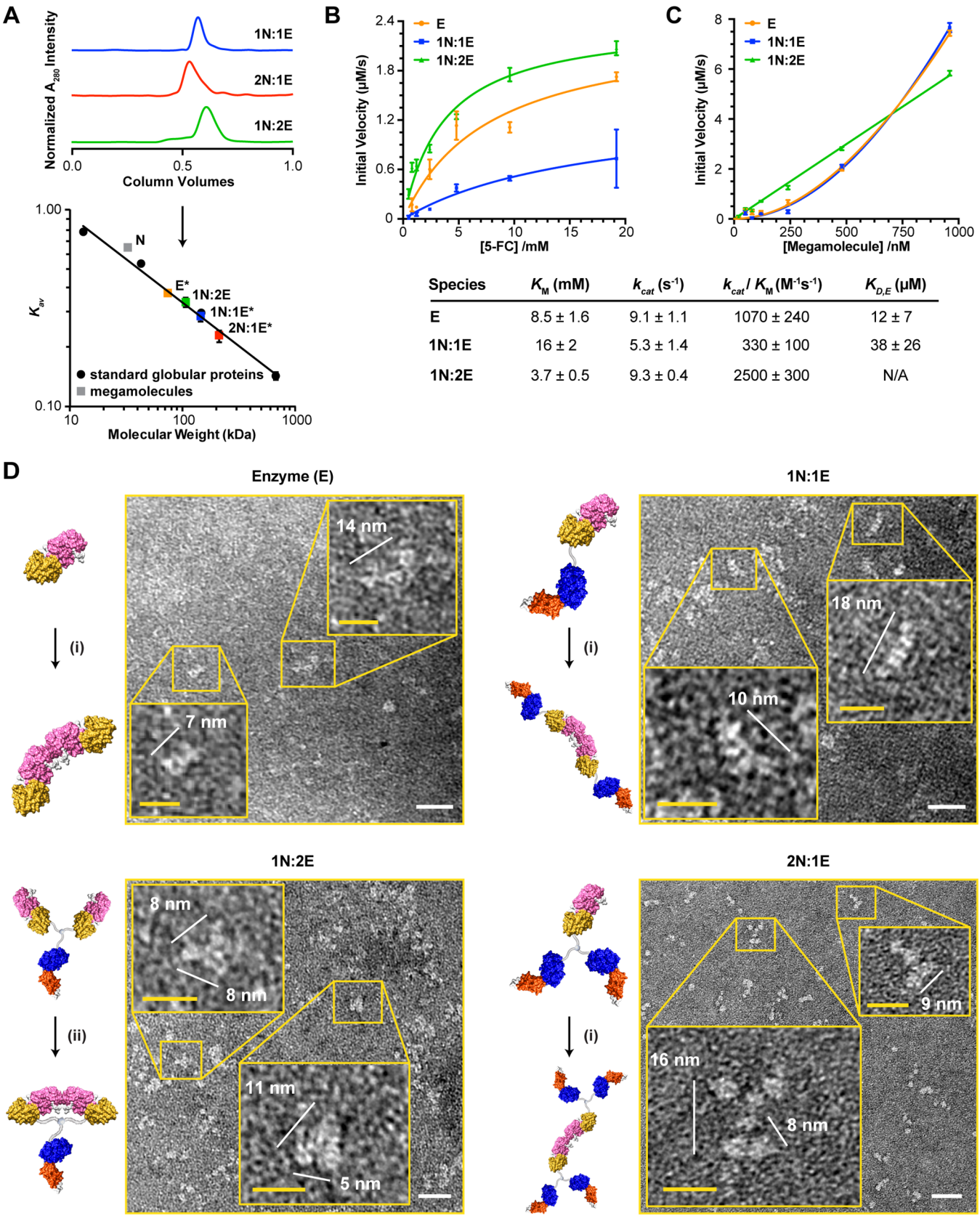

Species	K_M (mM)	k_{cat} (s^{-1})	k_{cat}/K_M ($M^{-1}s^{-1}$)	$K_{D,E}$ (μM)
E	8.5 ± 1.6	9.1 ± 1.1	1070 ± 240	12 ± 7
1N:1E	16 ± 2	5.3 ± 1.4	330 ± 100	38 ± 26
1N:2E	3.7 ± 0.5	9.3 ± 0.4	2500 ± 300	N/A

Figure 3. Characterization of yCD activity and nanobody−enzyme megamolecule structure. A. Size-exclusion chromatograms of megamolecule purification and SEC analyzed plot of partition coefficient (K_{av}) for megamolecules. *Assumes homodimer. B. Enzyme activity assay for E, 1N:1E, and 1N:2E by varying substrate concentration to determine the Michalis-Menten kinetic parameters. C. Enzyme activity assay for E, 1N:1E, and 1N:2E by varying enzyme concentration to determine the dissociation constant for homodimerization ($K_{D,E}$). The concentration of 5-FC was equal to 10 mM. B,C. The mean of 4 biologic replicates is plotted and the error bars represent standard error. Average values are tabulated with error reported as the standard error of fitting. D. TEM characterization. White scale bars in full images represent 20 nm. Yellow scale bar represents 10 nm for inset images.

https://dx.doi.org/10.1021/acs.bioconjchem.0c00578
Bioconjugate Chem. XXXX, XXX, XXX−XXX

Figure 3. continued

Structural images representing megamolecule structures with (i) intermolecular or (ii) intramolecular dimerization of E. The measurement error in all images is ±1 nm, to account for the resolution limit due to negative staining.

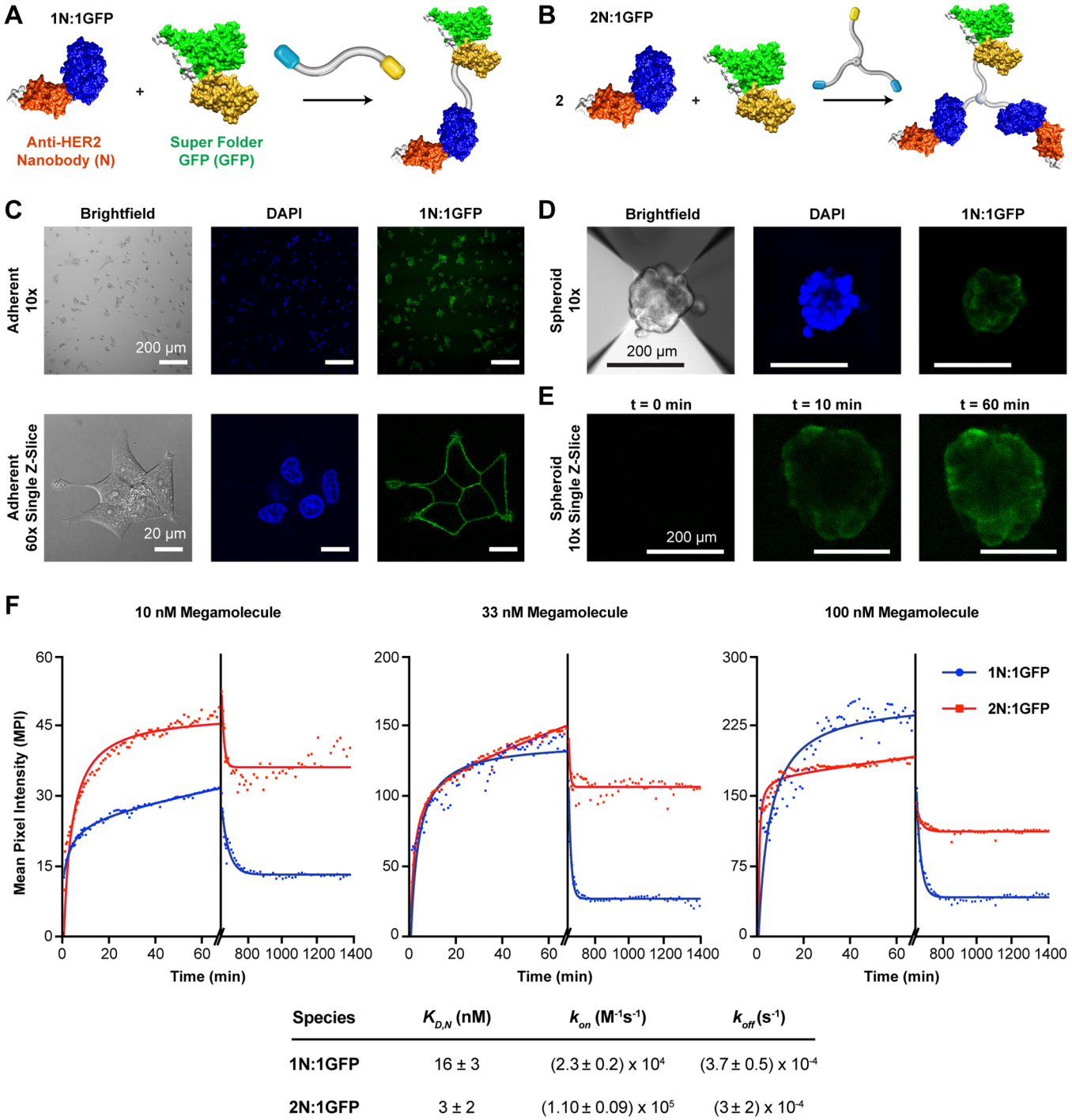

Species	$K_{D,N}$ (nM)	k_{on} ($M^{-1}s^{-1}$)	k_{off} (s^{-1})
1N:1GFP	16 ± 3	(2.3 ± 0.2) x 10^4	(3.7 ± 0.5) x 10^{-4}
2N:1GFP	3 ± 2	(1.10 ± 0.09) x 10^5	(3 ± 2) x 10^{-4}

Figure 4. Characterization of megamolecule binding. A,B. Synthetic schemes of fluorescent megamolecules with either A, one nanobody domain (1N:1GFP); or B, two nanobody domains (2N:1GFP) conjugated to a fusion protein containing a sfGFP domain. C. Adherent culture microscopy of BT-474 cells incubated with 10 nM 1N:1GFP after 2 h. Scale bars are 200 μm (top) and 20 μm (bottom). D,E. Spheroid culture confocal microscopy of BT-474 cells incubated with 50 nM 1N:1GFP. Scale bar is 200 μm. D. Image of spheroids after 2 h incubation with 1N:1GFP. E. Single *Z*-stack slice of spheroid center after a 1 h incubation with 1N:1GFP. F. Averages of fluorescence mean pixel intensity (MPI) of fixed adherent cells incubated with 1N:1GFP (blue) or 2N:1GFP (red) over time. After 80 min, the wells were washed three times and imaged to track dissociation from the cells. Curves for association (k_{on}) and dissociation (k_{off}) were fit from nonlinear fit kinetics software packages using GraphPad Prism from 7 to 9 biological replicates. Error reported as standard deviation.

https://dx.doi.org/10.1021/acs.bioconjchem.0c00578
Bioconjugate Chem. XXXX, XXX, XXX−XXX

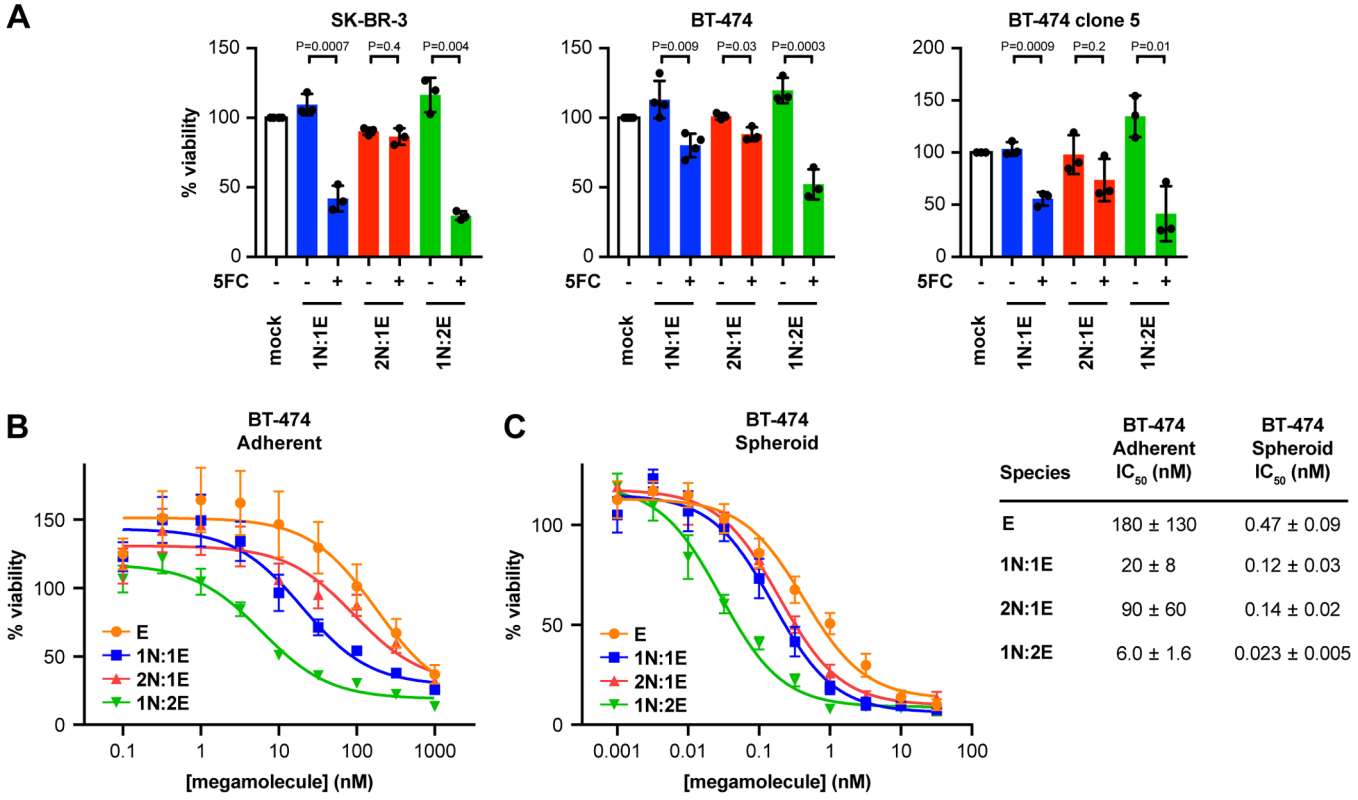

Figure 5. Cytotoxicity of multidomain nanobody−enzyme megamolecules. A. Cytotoxicity of adherent cultures with megamolecule prodrug therapy. A two-step protocol was used where first 10 nM megamolecule was incubated with cells, followed by washing to remove unbound megamolecules, and incubation with 5-FC. Mean values are plotted with error represented as 1 standard deviation. B,C. Megamolecule dose−response curves for the BT-474 cell line in B, adherent culture with washing; and C, spheroid culture without washing. All conditions were dosed with 4 mM 5-FC. Mean values are plotted with error represented as SEM. Table inset reports fitted values with standard error of fitting.

S12). The 1N:1GFP megamolecule first bound the outer cells of adherent BT-474 cell clusters, and over the period of a few minutes, the 1N:1GFP penetrated inner cells and cell−cell junctions (Figure 4C, Movie S1, Movie S2).

We next characterized the penetration of fluorescent megamolecules into spheroids. We treated BT-474 spheroids with the 1N:1GFP megamolecule for 2 h and used confocal microscopy to track the distribution of the megamolecule (Figure 4D). To assess penetration of the megamolecule in the spheroid, we generated *Z*-stack images at multiple time points. The megamolecule first saturated the cells on the spheroid surface, followed by penetration of 1N:1GFP between cells into the center of the spheroid (Figure 4E). We measured the penetration of 1N:1GFP in a 1000-cell spheroid (~0.01 mm^3) and found that 1N:1GFP reached the spheroid center after 1 h (Figure S13).

We repeated this experiment with a 2N:1GFP megamolecule—which serves as a surrogate for the 2N:1E megamolecule—to determine the effect of bivalent recognition on mass transport (Figure 4B and Figure S11). We measured the binding dynamics of both fluorescent megamolecules in adherent culture under both live and fixed conditions at various concentrations to determine the dose dependence of cell binding (Figure S14). As expected, the 2N:1GFP megamolecule bound more rapidly to the outer cells at low concentrations, while the 1N:1GFP megamolecule penetrated inner cells and cell−cell junctions more rapidly at high concentrations (Figure 4F, Figure S14, Movie S3). After 80 min of fluorescent megamolecule incubation, we washed away unbound megamolecules and tracked the loss of fluorescence over time. For all concentrations, 2N:1GFP remained bound to a greater extent after washing than did 1N:1GFP. We calculated the nanobody dissociation constant, $K_{D,N}$, for each megamolecule. The 1N:1GFP and 2N:1GFP megamolecules had $K_{D,N}$ values of 16 ± 3 nM and 3 ± 2 nM on fixed cells, respectively, which agreed well with the previously reported value of 4.12 ± 0.47 nM on the HER2+ human breast cancer cell line SKOV-3 cells.[44] Addition of a second binding domain increased the binding affinity 5-fold (Figure 4F), indicating an avidity effect in the 2N:1GFP megamolecule. These results show that the bivalent megamolecule had greater binding affinity, while the monovalent megamolecule exhibited faster penetration through cell−cell junctions to the center of the spheroid.

Cytotoxicity of Multidomain Nanobody−Enzyme Megamolecule Prodrug Treatment. We next tested the cytotoxicity of the three megamolecules in adherent culture to determine the effect of increasing the number of nanobody or enzyme domains (Figure 1B−D). All megamolecules elicited a cytotoxic effect by enzymatically activating 5-FC (Figure 5A). The cytotoxic effect of 1N:2E was greater than 1N:1E for the more sensitive cell line (SK-BR-3). We then assessed the dose-dependence of megamolecules on cytotoxicity in adherent culture (Figure 5B and Figures S15−S16). The IC_{50} for the 1N:2E megamolecule was 3-fold lower relative to the 1N:1E megamolecule for BT-474. Increasing the number of nanobody domains in the 2N:1E megamolecule increased the IC_{50} 4-fold relative to the 1N:1E megamolecule for BT-474. Thus, increasing the number of enzyme domains in a single

https://dx.doi.org/10.1021/acs.bioconjchem.0c00578
Bioconjugate Chem. XXXX, XXX, XXX−XXX

megamolecule increased the cytotoxicity of megamolecule prodrug therapy.

Finally, we tested megamolecule prodrug cytotoxicity in spheroid cultures. Because tumor spheroids rest on the bottom of the culture dish, a washing protocol was not used. Instead, we compared the cytotoxicity of the three megamolecules to the E fusion protein. The E fusion protein prodrug treatment represented activation of 5-FC in the bulk media, because the E fusion protein did not bind to cells (Figure 2E,F). We then characterized the effect of local activation of 5-FC by comparing cytotoxicity from bulk enzymatic activation with cell-localized enzymatic activation (Figure 5C and Figure S16). Compared to E fusion protein prodrug treatment, the 1N:1E megamolecule was more cytotoxic (4-fold decrease in IC_{50} for BT-474) (Figure 3B). The 2N:1E megamolecule was more cytotoxic than the E fusion protein and had a similar cytotoxicity to the 1N:1E megamolecule. The 1N:2E megamolecule was more cytotoxic than both E fusion protein and the other megamolecules. The megamolecule IC_{50} of the 1N:2E megamolecule was 20-fold lower than E fusion protein and 5-fold lower than the 1N:1E megamolecule.

DISCUSSION

Next-generation biologics that combine advances in protein conjugation and nanotechnology are leading to new classes of therapeutics to treat cancer.[45,46] A primary, though still challenging, goal is the control of structure and homogeneity of biologics, ultimately producing therapeutics of a uniform composition. In this paper, we show how the megamolecule approach can be used to prepare covalent protein nanostructures that are perfectly defined and that allow for precise organization of multiple functional domains, in ways that are important to tuning cell binding strength and drug activation rate. The modular assembly of megamolecules based on the efficient reactions of cutinase or SnapTag with linkers[13,14] will allow the development of new structures to target other tumor-specific antigens or different enzyme activities with control over both the domain type and number.

We programmed the megamolecule structure by varying the number of functional protein domains, which had distinct effects on their solution-phase behavior, enzyme activity, and cell binding strength. Previous studies have not explicitly addressed the role of dimerization of yCD in its activity. In this work, we designed molecules that had two copies of the enzyme, where the structure enforced intramolecular dimerization of the homodimeric yCD (Figure 3). Compared to the 1N:1E megamolecule, the 1N:2E megamolecule showed an 8-fold improvement in the catalytic efficiency (Figure 3B) and a 3- and 5-fold improvement in cytotoxicity for the BT-474 cell line in adherent and spheroid culture, respectively (Figure 5B,C). This enhancement cannot be fully explained by the increased number of enzyme domains in a single molecule, as the 1N:2E megamolecule is still 2-fold more cytotoxic in both culture formats when calculating concentration on a per enzyme domain basis. In contrast, the 1N:1E and 2N:1E megamolecules had a single enzyme domain and therefore dimerized intermolecularly, leading to lowered enzyme activity and reduced cytotoxicity. We also compared the binding kinetics of multinanobody domain megamolecules to the HER2+ BT-474 cell line in live cell culture using confocal microscopy. We synthesized fluorescent megamolecules having either one or two anti-HER2 nanobody domains to allow optical tracking of the dynamics of cell binding and spheroid penetration. The presence of a second nanobody domain in the megamolecule resulted in more avid cell binding, as shown by a 5-fold reduction in the dissociation constant. We also observed that the second nanobody domain led to slower penetration into the spheroid, again likely due to the tighter binding of this molecule to the cell surface.[47,48] Clearly, the synthetic control that the megamolecule approach offers over the number of domains is important to optimizing the design of antibody-directed enzyme prodrug therapy.

Tumors can be characterized by different levels of antigens on the cell surface, and it is expected that the density will affect their sensitivity to antibody therapeutics. Moreover, within a tumor, there is substantial heterogeneity that will influence the efficacy of a therapeutic. For example, in HER2+ breast tumors more than 30% of the cancer cells have threshold levels of the receptor,[49] reflecting the significant heterogeneity within the HER2+ subtype.[50] Hence, we had evaluated our megamolecules against three HER2+ and two HER2- cell lines to determine whether the activity was cell type-specific. We found that the 1N:1E megamolecule was sufficiently cytotoxic for the SK-BR-3 cell line, which is known to be very sensitive to 5-FU. However, this megamolecule was poorly active in the trastuzumab-resistant cell line BT-474 clone 5, but the 1N:2E megamolecule did display a strong cytotoxic response in this cell line. These results again suggest that the ability to control the number and organization of enzyme domains synthetically can tune the cytotoxicity of the nanobody−enzyme megamolecule in a heterogeneous tumor.

The numbers and identities of domains, and their structural organization within a molecule, certainly play a significant role in the activity of antibody-mimic therapeutics. Difficulties in the preparation of uniform molecules have largely prevented studies that reveal structure−activity relationships. The megamolecule approach is exciting because its modular synthesis allows nearly unlimited control over the design of homogeneous antibody scaffolds with unique topology, multispecificity, and multivalency. In this work, we demonstrated how both the stoichiometry of the enzyme domain—which dimerizes and has greater activity with two copies in the molecule—and the nanobody have an important role in localized, cell-specific activity. We believe this approach will be valuable in elucidating the structure−activity design rules in a number of other antibody-based contexts.

ASSOCIATED CONTENT

Supporting Information

The Supporting Information is available free of charge at https://pubs.acs.org/doi/10.1021/acs.bioconjchem.0c00578.

SI Materials and Methods provide a full description of cloning, protein expression and purification, linker synthesis, cell culture, megamolecule synthesis and characterization, flow cytometry, and assays of activity, binding, and cell viability (PDF)

Movie S1. Time-lapse (1 hour) 10× overview for 1 hour of 50 nM 1N:1GFP megamolecules binding to adherent BT-474 cells (live-cell confocal microscopy) (MOV)

Movie S2. Time-lapse (1 hour) 60× single Z-slide view of 50 nM 1N:1GFP megamolecules binding between cell-cell junctions in adherent BT-474 cells (live-cell confocal microscopy) (MOV)

Movie S3. Time-lapse (1 hour) 60× single Z-slide view of 10 nM 1N:1GFP megamolecules penetrating into a 1000

https://dx.doi.org/10.1021/acs.bioconjchem.0c00578
Bioconjugate Chem. XXXX, XXX, XXX−XXX

cell BT-474 spheroid (live-cell confocal microscopy) (MOV)

AUTHOR INFORMATION

Corresponding Author

Milan Mrksich − *Department of Biomedical Engineering and Department of Chemistry, Northwestern University, Evanston, Illinois 60208, United States;* orcid.org/0000-0002-4964-796X; Email: milan.mrksich@northwestern.edu

Authors

Kevin J. Metcalf − *Department of Anatomy, University of California, San Francisco, San Francisco, California 94143, United States; Department of Biomedical Engineering, Northwestern University, Evanston, Illinois 60208, United States;* orcid.org/0000-0002-2721-3378

Blaise R. Kimmel − *Department of Chemical and Biological Engineering, Northwestern University, Evanston, Illinois 60208, United States;* orcid.org/0000-0002-9582-9887

Daniel J. Sykora − *Department of Biomedical Engineering, Northwestern University, Evanston, Illinois 60208, United States;* orcid.org/0000-0002-5675-7454

Justin A. Modica − *Department of Biomedical Engineering, Northwestern University, Evanston, Illinois 60208, United States;* orcid.org/0000-0002-3218-7311

Kelly A. Parker − *Department of Materials Science and Engineering, Northwestern University, Evanston, Illinois 60208, United States*

Eric Berens − *Department of Anatomy, University of California, San Francisco, San Francisco, California 94143, United States*

Raymond Dai − *Department of Chemistry, Northwestern University, Evanston, Illinois 60208, United States*

Vinayak P. Dravid − *Department of Materials Science and Engineering, Northwestern University, Evanston, Illinois 60208, United States;* orcid.org/0000-0002-6007-3063

[#]**Zena Werb** − *Department of Anatomy, University of California, San Francisco, San Francisco, California 94143, United States;* orcid.org/0000-0002-6525-3872

Complete contact information is available at: https://pubs.acs.org/10.1021/acs.bioconjchem.0c00578

Author Contributions

[†]K.J.M. and B.R.K. contributed equally.

Notes

The authors declare no competing financial interest.
[#]Deceased June 16, 2020

ACKNOWLEDGMENTS

K.J.M. acknowledges support from the NIH/NCI training grant T32 CA186897 and an American Cancer Society−2017 Seattle Gala Paddle Raise Postdoctoral Fellowship, PF-18-118-01-CDD. B.R.K. and K.A.P. acknowledge support from the Ryan Fellowship, the International Institute for Nanotechnology at Northwestern University, and the National Science Foundation Graduate Research Fellowship under Grant DGE-1842165. Research reported in this publication was supported by AFRL FA8650-15-2-5518, ARO MURI FA9550-16-1-0150, and from the National Cancer Institute of the National Institutes of Health under Award Numbers U54CA199091and U01CA199315. This work made use of the BioCryo facility of Northwestern University's NUANCE Center, which has received support from the Soft and Hybrid Nanotechnology Experimental (SHyNE) Resource (NSF ECCS-1542205); and made use of facilities partially supported by the MRSEC program (NSF DMR-1720139) at the Materials Research Center.

REFERENCES

(1) Sharma, S. K., and Bagshawe, K. D. (2017) Antibody Directed Enzyme Prodrug Therapy (ADEPT): Trials and tribulations. *Adv. Drug Delivery Rev. 118*, 2−7.

(2) Bagshawe, K. D. (2006) Antibody-directed enzyme prodrug therapy (ADEPT) for cancer. *Expert Rev. Anticancer Ther. 6*, 1421−1431.

(3) Singh, Y., Palombo, M., and Sinko, P. J. (2008) Recent Trends in Targeted Anticancer Prodrug and Conjugate Design. *Curr. Med. Chem. 15*, 1802−1826.

(4) Senter, P. D., and Springer, C. J. (2001) Selective activation of anticancer prodrugs by monoclonal antibody−enzyme conjugates. *Adv. Drug Delivery Rev. 53*, 247−264.

(5) Melton, R. G., and Sherwood, R. F. (1996) antibody−enzyme Conjugates for Cancer Therapy. *J. Natl. Cancer Inst 88*, 153−165.

(6) Bagshawe, P. K. D. (2007) Antibody-Directed Enzyme Prodrug Therapy, in *Prodrugs, Biotechnology: Pharmaceutical Aspects* (Stella, V. J.,et al., Eds.) pp 525−540, Springer New York.

(7) Baslé, E., Joubert, N., and Pucheault, M. (2010) Protein Chemical Modification on Endogenous Amino Acids. *Chem. Biol. 17*, 213−227.

(8) Patterson, D. M., Nazarova, L. A., and Prescher, J. A. (2014) Finding the Right (Bioorthogonal) Chemistry. *ACS Chem. Biol. 9*, 592−605.

(9) McKay, C. S., and Finn, M. G. (2014) Click Chemistry in Complex Mixtures: Bioorthogonal Bioconjugation. *Chem. Biol. 21*, 1075−1101.

(10) Kim, C. H., Axup, J. Y., Dubrovska, A., Kazane, S. A., Hutchins, B. A., Wold, E. D., Smider, V. V., and Schultz, P. G. (2012) Synthesis of Bispecific Antibodies using Genetically Encoded Unnatural Amino Acids. *J. Am. Chem. Soc. 134*, 9918−9921.

(11) Modica, J. A., Skarpathiotis, S., and Mrksich, M. (2012) Modular Assembly of Protein Building Blocks To Create Precisely Defined Megamolecules. *ChemBioChem 13*, 2331−2334.

(12) Modica, J. A., Lin, Y., and Mrksich, M. (2018) Synthesis of Cyclic Megamolecules. *J. Am. Chem. Soc. 140*, 6391−6399.

(13) Taylor, E. L., Metcalf, K. J., Carlotti, B., Modica, J. A., Schatz, G. C., Mrksich, M., and Goodson, T., III (2018) Long-Range Energy Transfer in Protein Megamolecules. *J. Am. Chem. Soc. 140*, 15731−15743.

(14) Modica, J. A., Iderzorig, T., and Mrksich, M. (2020) Design and Synthesis of Megamolecule Mimics of a Therapeutic Antibody. *J. Am. Chem. Soc. 142*, 13657−13661.

(15) Zhang, X., Li, X., You, Q., and Zhang, X. (2017) Prodrug strategy for cancer cell-specific targeting: A recent overview. *Eur. J. Med. Chem. 139*, 542−563.

(16) Pruszynski, M., Koumarianou, E., Vaidyanathan, G., Revets, H., Devoogdt, N., Lahoutte, T., and Zalutsky, M. R. (2013) Targeting breast carcinoma with radioiodinated anti-HER2 Nanobody. *Nucl. Med. Biol. 40*, 52−59.

(17) Cortez-Retamozo, V., Backmann, N., Senter, P. D., Wernery, U., De Baetelier, P., Muyldermans, S., and Revets, H. (2004) Efficient Cancer Therapy with a Nanobody-Based Conjugate. *Cancer Res. 64*, 2853−2857.

(18) Kijanka, M., Dorresteijn, B., Oliveira, S., and van Bergen en Henegouwen, P. M. P. (2015) Nanobody-based cancer therapy of solid tumors. *Nanomedicine (London, U. K.) 10*, 161−174.

(19) Xiao, H., Woods, E. C., Vukojicic, P., and Bertozzi, C. R. (2016) Precision glycocalyx editing as a strategy for cancer immunotherapy. *Proc. Natl. Acad. Sci. U. S. A. 113*, 10304−10309.

(20) Gray, M. A., Stanczak, M. A., Mantuano, N. R., Xiao, H., Pijnenborg, J. F. A., Malaker, S. A., Miller, C. L., Weidenbacher, P. A., Tanzo, J. T., Ahn, G., Woods, E. C., Läubli, H., and Bertozzi, C. R. (2020) Targeted Glycan Degradation Potentiates the Anticancer Immune Response in Vivo. *Nat. Chem. Biol. 16* (16), 1376−1384.

(21) Levengood, M. R., Zhang, X., Hunter, J. H., Emmerton, K. K., Miyamoto, J. B., Lewis, T. S., and Senter, P. D. (2017) Orthogonal Cysteine Protection Enables Homogeneous Multi-Drug Antibody–Drug Conjugates. *Angew. Chem., Int. Ed. 56*, 733–737.
(22) Ishihara, J., Fukunaga, K., Ishihara, A., Larsson, H. M., Potin, L., Hosseinchi, P., Galliverti, G., Swartz, M. A., and Hubbell, J. A. (2017) Matrix-binding checkpoint immunotherapies enhance antitumor efficacy and reduce adverse events. *Sci. Transl. Med. 9*, No. eaan0401.
(23) Ishihara, J., Ishihara, A., Sasaki, K., Lee, S. S. Y., Williford, J. H., Yasui, M., Abe, H., Potin, L., Hosseinchi, P., Fukunaga, K., et al. (2019) Targeted antibody and cytokine cancer immunotherapies through collagen affinity. *Sci. Transl. Med. 11*, No. eaau3259.
(24) Srikun, D., Albers, A. E., Nam, C. I., Iavarone, A. T., and Chang, C. J. (2010) Organelle-Targetable Fluorescent Probes for Imaging Hydrogen Peroxide in Living Cells via SNAP-Tag Protein Labeling. *J. Am. Chem. Soc. 132*, 4455–4465.
(25) Hodneland, C. D., Lee, Y.-S., Min, D.-H., and Mrksich, M. (2002) Selective immobilization of proteins to self-assembled monolayers presenting active site-directed capture ligands. *Proc. Natl. Acad. Sci. U. S. A. 99*, 5048–5052.
(26) Mollwitz, B., Brunk, E., Schmitt, S., Pojer, F., Bannwarth, M., Schiltz, M., Rothlisberger, U., and Johnsson, K. (2012) Directed Evolution of the Suicide Protein O^6-Alkylguanine-DNA Alkyltransferase for Increased Reactivity Results in an Alkylated Protein with Exceptional Stability. *Biochemistry 51*, 986–994.
(27) Kievit, E., Bershad, E., Eg, E., Sethna, P., Dev, I., Lawrence, T. S., and Rehemtulla, A. (1999) Superiority of Yeast over Bacterial Cytosine Deaminase for Enzyme/Prodrug Gene Therapy in Colon Cancer Xenografts. *Cancer Res. 59*, 1417–1421.
(28) Kimmel, B., Modica, J., Parker, K., Dravid, V., and Mrksich, M. (2020) Solid-Phase Synthesis of Megamolecules. *J. Am. Chem. Soc. 142*, 4534–4538.
(29) Subik, K., Lee, J. F., Baxter, L., Strzepek, T., Costello, D., Crowley, P., Xing, L., Hung, M. C., Bonfiglio, T., Hicks, D. G., et al. (2010) The Expression Patterns of ER, PR, HER2, CK5/6, EGFR, Ki-67 and AR by Immunohistochemical Analysis in Breast Cancer Cell Lines. *Breast Cancer: Basic Clin. Res. 4*, 35–41.
(30) Kute, T., Lack, C. M., Willingham, M., Bishwokama, B., Williams, H., Barrett, K., Mitchell, T., and Vaughn, J. P. (2004) Development of Herceptin resistance in breast cancer cells. *Cytometry 57A*, 86–93.
(31) Kim, J. B. (2005) Three-dimensional tissue culture models in cancer biology. *Semin. Cancer Biol. 15*, 365–377.
(32) Nath, S., and Devi, G. R. (2016) Three-dimensional culture systems in cancer research: Focus on tumor spheroid model. *Pharmacol. Ther. 163*, 94–108.
(33) Su, Y.-L., and Hu, S.-H. (2018) Functional Nanoparticles for Tumor Penetration of Therapeutics. *Pharmaceutics 10*, 193.
(34) Sawicki, L. A., Ovadia, E. M., Pradhan, L., Cowart, J. E., Ross, K. E., Wu, C. H., and Kloxin, A. M. (2019) Tunable synthetic extracellular matrices to investigate breast cancer response to biophysical and biochemical cues. *APL Bioeng 3*, 016101.
(35) Ivascu, A., and Kubbies, M. (2007) Diversity of cell-mediated adhesions in breast cancer spheroids. *Int. J. Oncol. 31*, 1403–1413.
(36) Imamura, Y., et al. (2015) Comparison of 2D- and 3D-culture models as drug-testing platforms in breast cancer. *Oncol. Rep. 33*, 1837–1843.
(37) Balalaeva, I. V., Sokolova, E. A., Puzhikhina, A. D., Brilkina, A. A., and Deyev, S. M. (2017) Spheroids of HER2-Positive Breast Adenocarcinoma for Studying Anticancer Immunotoxins In Vitro. *Acta Naturae 9*, 38–43.
(38) Senter, P. D., Su, P. C. D., Katsuragi, T., Sakai, T., Cosand, W. L., Hellstrom, I., and Hellstrom, K. E. (1991) Generation of 5-fluorouracil from 5-fluorocytosine by monoclonal antibody-cytosine deaminase conjugates. *Bioconjugate Chem. 2*, 447–451.
(39) Yao, L., Li, Y., Wu, Y., Liu, A., and Yan, H. (2005) Product Release Is Rate-Limiting in the Activation of the Prodrug 5-Fluorocytosine by Yeast Cytosine Deaminase. *Biochemistry 44*, 5940–5947.
(40) Kumar, R. P., Morehouse, B. R., Fofana, J., Trieu, M. M., Zhou, D. H., Lorenz, M. O., and Oprian, D. D. (2017) Structure and monomer/dimer equilibrium for the guanylyl cyclase domain of the optogenetics protein RhoGC. *J. Biol. Chem. 292*, 21578–21589.
(41) Cheng, S.-C., Chang, G.-G., and Chou, C.-Y. (2010) Mutation of Glu-166 Blocks the Substrate-Induced Dimerization of SARS Coronavirus Main Protease. *Biophys. J. 98*, 1327–1336.
(42) Gallagher, J. R., Kim, A. J., Gulati, N. M., and Harris, A. K. (2019) Negative-Stain Transmission Electron Microscopy of Molecular Complexes for Image Analysis by 2D Class Averaging. *Curr. Protoc Microbiol 54*, No. e90.
(43) Pédelacq, J.-D., Cabantous, S., Tran, T., Terwilliger, T. C., and Waldo, G. S. (2006) Engineering and characterization of a superfolder green fluorescent protein. *Nat. Biotechnol. 24*, 79–88.
(44) Pruszynski, M., D'Huyvetter, M., Bruchertseifer, F., Morgenstern, A., and Lahoutte, T. (2018) Evaluation of an Anti-HER2 Nanobody Labeled with 225Ac for Targeted α-Particle Therapy of Cancer. *Mol. Pharmaceutics 15*, 1457–1466.
(45) Agarwal, P., and Bertozzi, C. R. (2015) Site-Specific Antibody–Drug Conjugates: The Nexus of Bioorthogonal Chemistry, Protein Engineering, and Drug Development. *Bioconjugate Chem. 26*, 176–192.
(46) Kintzing, J. R., Filsinger Interrante, M. V., and Cochran, J. R. (2016) Emerging Strategies for Developing Next-Generation Protein Therapeutics for Cancer Treatment. *Trends Pharmacol. Sci. 37*, 993–1008.
(47) Ackerman, M. E., Pawlowski, D., and Wittrup, K. D. (2008) Effect of antigen turnover rate and expression level on antibody penetration into tumor spheroids. *Mol. Cancer Ther. 7*, 2233–2240.
(48) Graff, C. P., and Wittrup, K. D. (2003) Theoretical Analysis of Antibody Targeting of Tumor Spheroids. *Cancer Res. 63*, 1288–1296.
(49) Wolff, A. C., Hammond, M. E. H., Schwartz, J. N., Hagerty, K. L., Allre, D. C., Cote, R. J., Dowsett, M., Fitzgibbons, P. L., Hanna, W. M., Langer, A., et al. (2007) American Society of Clinical Oncology/College of American Pathologists Guideline Recommendations for Human Epidermal Growth Factor Receptor 2 Testing in Breast Cancer. *Arch Pathol Lab Med. 131*, 18–43.
(50) Rivenbark, A. G., O'Connor, S. M., and Coleman, W. B. (2013) Molecular and Cellular Heterogeneity in Breast Cancer: Challenges for Personalized Medicine. *Am. J. Pathol. 183*, 1113–1124.

https://dx.doi.org/10.1021/acs.bioconjchem.0c00578
Bioconjugate Chem. XXXX, XXX, XXX–XXX